BIOCHEMISTRY

Promotion of row 1–specific tip complex condensates by Gpsm2-Gαi provides insights into row identity of the tallest stereocilia

Yingdong Shi[1]†, Lin Lin[2]†, Chao Wang[1]*, Jinwei Zhu[2]*

Copyright © 2022 The Authors, some rights reserved; exclusive licensee American Association for the Advancement of Science. No claim to original U.S. Government Works. Distributed under a Creative Commons Attribution NonCommercial License 4.0 (CC BY-NC).

The mechanosensory stereocilia in hair cells are organized into rows of graded height, a property crucial for auditory perception. Gpsm2-Gαi-Whirlin-Myo15-Eps8 complex at tips of the tallest stereocilia is proposed to define hair bundle row identity, although the underlying mechanism remains elusive. Here, we find that Gpsm2 could undergo phase separation. Moreover, row 1–specific Gpsm2-Gαi complex significantly promotes the formation of the five-component tip complex density (5xTCD) condensates. The 5xTCD condensates display much stronger actin-bundling ability than those without Gpsm2-Gαi, which may provide critical insights into how Gpsm2-Gαi specifies the tallest stereocilia. A deafness-associated mutation of Gpsm2 leads to impaired formation of the 5xTCD condensates and consequently reduced actin bundling, providing possible clues for etiology of hearing loss in patients with Chudley-McCullough syndrome.

INTRODUCTION

S dde ec e e hee he a echa e ha ce he ch ea f e ea. The echa ca e e ga e e f ha ce a e e e c a, ac e fac - ch a he a ca face (*1*, *2*). S e e c a a e e c ec ed b e e a d f ha b d e ch a (*3*, *4*). A e c a fea- e f e e c a ha he a e ga ed f g aded he gh (*5*) (F g. 1A). S ch a a ca e- e a e c ca f ech- a e a d c . Mecha ca f ce e ed b d a e e e e c a defec a d he a e , h ch, , ac a e he echa e ec ca a d ce cha e ca ed he h e e e c a, h ach e g he echa e ec ca a - d c (*1*, *6*).

P e de e e f e e c a e e a f a d e- ce , a a fe ed b e e e hea g ca ed b ge e c - a fge e ha eg a e e e c ag h (*2*, *4*). Ma f he e ge e e c de ac c e e eg a e ha ca e a he e e c -de e a ea f he d a f e e c a (*7*, *8*), a g c ca e gac e a a db d g. E - a e a e Wh , 15 (M 15), a d e de a g h fac- ece a h a b a e 8 (E 8) (*9* *11*). M ce def c e a f he e h ee ge e e h b ed a e e c a g a d - f d deaf e (*10*, *12*, *13*). Mecha ca , ea d he de - a ed ha he h ee e ca d ec e ac h e a he f a gh c e (*14*, *15*) (F g. 1B). The e e ac a M 15 a e ca g (Wh a d E 8) h- de e g e e c a he e E 8, a e a c e ed c e e a effec , e ec e ac -ca g a d ac -b d g ac e (*9*). M e e, he e a c e f d- d ha e e a a (LLPS) a d g ce a d fac a e ac b d g, d ca g ha he e ec -de e a ea ca ed a he f e e c a a f a LLPS f he c e a (*14*).

H e e, e a ce a h e e c a ad cha a ca e- e a ch ec e a d ha de e e he de f he a e e e c a. G e he a a a e e he a ca e a e f e e c a, ece de a a ce a a - de c c a c e f he be de g echa (*16* *20*). A c e f I c eab e (I c), G e g a g d a 2 (G 2; a a LGN), a d he e e c G e Gα (.e., I c-G 2-Gα c e) def e a a ca c a e (e ed a he ba e e) h a ha c e c b d- a a g he ed a e a a a a c ea e he V- ha ed ha b d e (*16*). M ab G 2-Gα he e c ed e- ched a he d a f e e c a ab g he ba e e ha a e bec e he a e (1), c ca ed h Wh , M 15, a d E 8 (*18*, *21*) (F g. 1A). M ce def c e *Gpsm2* *Gnai* (e c d- gGα) h ed a e e c a ga d e e e hea g a *whirler* ce (ac a g Wh), *shaker-2* ce (ac g M 15), a d *Eps8*- c ce d d (*18*, *22* *24*). Rece , a *Gpsm2* e e f d a e h Ch d e-McC gh d e (CMCS; O e Me de a I he a ce Ma : 604213), a a e a - a ece e d ea e cha ac e ed b e e e f d e - e a hea g a d a a age e f he c ca (*25* *27*). M e e, G 2 a f d e ac h Wh d ec c - ca ed a h gh de e a d a h a ca - e c e a he f he a e e e c a (*23*). The ef e, he f ec - e (M 15, E 8, Wh , G 2, a d Gα) a he f he a e e e c a a e a e he a e a h a de e e he de a h gh he de g echa a ge ce a. I h d , e cha ac e e he G 2-Wh e ac de a h gh ac b a f b che ca a d b h ca a - ache . We f d ha G 2 e fc d f LLPS a d ce . G 2-Gα g f ca e he f a f he f e- c e c e de (5 TCD) c de a e (G 2-Gα - Wh -M 15-E 8). The effec e de G 2 LLPS, a a a f G 2 ha d LLPS a ge a he 5 TCD c de a e f a . C e h he

[1]Department of Neurology, the First Affiliated Hospital of USTC, Ministry of Education Key Laboratory for Cellular Dynamics, Biomedical Sciences and Health Laboratory of Anhui Province, School of Life Sciences, Division of Life Sciences and Medicine, University of Science and Technology of China, Hefei 230027, China. [2]Bio-X Institutes, Key Laboratory for the Genetics of Developmental and Neuropsychiatric Disorders, Ministry of Education, Shanghai Jiao Tong University, Shanghai 200240, China.
*Corresponding author. Email: cwangust@ustc.edu.cn (C.W.); jinwei.zhu@sjtu.edu.cn (J.Z.)
†These authors contributed equally to this work.

Downloaded from https://www.science.org at Shanghai Jiao Tong University on June 23, 2022

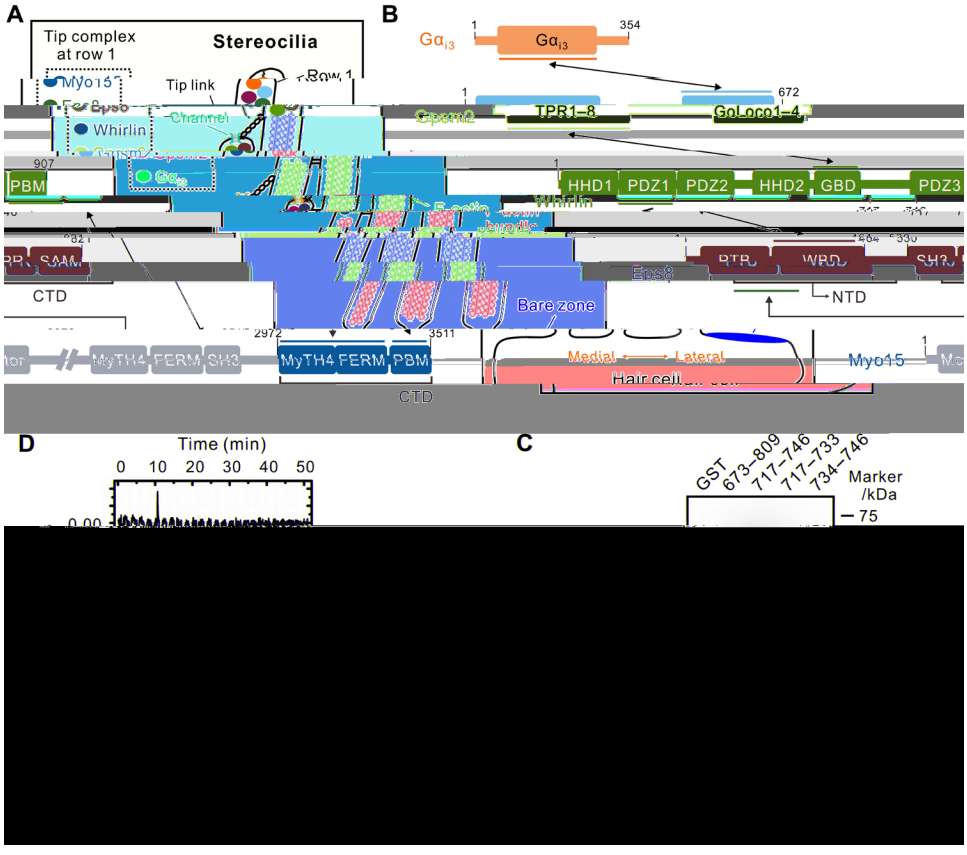

Fig. 1. The Gpsm2-Whirlin interaction. (**A**) A schematic diagram illustrating the organization of hair cell stereocilia. An apical compartment (termed as the "bare zone") with a sharp microvilli exclusion boundary along the mediolateral planar polarity axis is highlighted with a blue area. The five-component tip complex is also shown. (**B**) Domain organizations of key components of the tip complex in stereocilia. The two-way arrows indicate direct interactions. TPR, tetratricopeptide repeat; HHD, harmonin homology domain; PDZ, PSD-95/Discs-large/ZO-1 homology; PBM, PDZ binding motif; PTB, phosphotyrosine binding; WBD, Whirlin binding domain; SH3, src homology 3; PR, proline-rich region; SAM, sterile alpha motif; MyTH4, myosin tail homology 4; FERM, 4.1/ezrin/radixin/moesin; GBD, Gpsm2-binding domain; NTD, N-terminal domain; CTD, C-terminal domain. Note that $Eps8^{NTD}$ contains PTB and WBD domains; $Eps8^{CTD}$ contains SH3, PR, and SAM domains with actin-bundling activity. $Myo15^{CTD}$ contains C-terminal MyTH4, FERM, and PBM domains, amino acids 2972 to 3511. $Myo15^{CTD}$ was used in the in vitro condensate reconstitution assays. (**C**) GST pull-down assays showing that the minimal GBD on Whirlin is the fragment encompassing amino acids 717 to 746. $Gpsm2^{TPR}$: amino acids 15 to 350; IB, immunoblot. (**D**) ITC assay showing the binding affinity between $Gpsm2^{TPR}$ and $Whirlin^{GBD}$.

LLPS ca ab e, 5 TCD c de a e d a ch ge ac - b d g ab ha M 15-E 8 a d Wh -M 15-E 8 d, h ch a de c ca gh h G 2-Gα ec fe he a e e e c aa d def e ha b d e de N ab , a CMCS-a c a ed a f G 2 e fe e h he c de - a e f a a d c e e a ac b d g, ffe g b e c e f he e g f CMCS- e a ed hea g .

RESULTS

Characterization of the Gpsm2-Whirlin interaction

G 2-Gα e e Wh a a ada each he f he a e e e c aa d f he M 15-E 8-Wh -G 2-Gα c e ec f c 1 (*21*). We f e d ec he e ac be ee G 2 a d Wh . P e e h ed ha a f ag e f Wh [a ac d 672 810] e ac ed h N- e a d - a f G 2 (*23*). G 2 c a e gh e a c e de e ea (TPR) a N e [he ea f e G 2^{TPR} (a ac d 15 350)] a d f G L c (GL) f a C e (F g. 1B). D g c d e e a fa e cce d , G 2 e e a a ada g he d e e a ach e h he c ca a c e( ) b b d g I ca d he c ea c a a a (N MA) a TPR a d Gα a GL, e ec e (*28*). We c f ed he G 2-Wh e ac b h g ha g - a h e *S*- a fe a e (GST) Wh $^{673\ 809}$ effec e b d f ed G 2^{TPR} (F g. 1C). F he ca -ba ed b d' ga a d ca ed ha Wh $^{717\ 746}$ (he ea f e Wh ^{GBD}, h f G 2-b d g d a) a ff c e a d ece a f G 2^{TPR} b d g, a f he de e f Wh ^{GBD} e he a N e (Wh $^{737\ 746}$) C e (Wh $^{717\ 733}$) d hed he b d g (F g. 1C). M e- e, he a a ca e (ITC) ba ed a a gh gh f ed e h ed ha G 2^{TPR} b d Wh ^{GBD} h a d c a c a (K_d) f 1.4 μM (F g. 1D).

Gpsm2-Whirlin complex structure

T ga gh he a e b c e f he G 2-Wh c e, e ed c a e a ch e c c c h ch Wh ^{GBD} a f ed C- e a G 2^{TPR}. We e e ab e b a c a f he ch e a d ff ac g 2.6- e . We ed he c e c eb ec a e ace e a d ef ed

Downloaded from https://www.science.org at Shanghai Jiao Tong University on June 23, 2022

a R_{free} f 28.3 a d a R_{work} f 23.1 (ab e S1). The f a c- e c de he e e e g h f G 2^{TPR} a d a ac d 729 743 f Wh .

I he c e c e, G 2^{TPR} f d a a gh -ha ded e- he c ea g a e c ca e g e ha h d he e e ded Wh^{GBD} e de a a a a e a e (F g. 2, A a d B). Each TPR e ea c f he ce , αA a d αB, c ec ed b a h (F g. 2A). The e gh TPR ac ge he f a c ed α-he ca e d, h αA he ce fac g he e face c ac- g he e ga ed Wh^{GBD} e de (F g. 2A). I ed ha he e a c f a f he a e b e ce f h e f G 2^{TPR} c e h he a e ch a N MA, I c, a d Afad (f g. S1) (*29 32*).

The Gpsm2-Whirlin interface

The G 2^{TPR}-Wh^{GBD} e face a ed a ed b ec- a c e ac a d h d ge b d g e ac . R221/R236 a d K106 f G 2^{TPR} f a b dge h E732^{Wh} a d D734^{Wh} , e ec e (F g. 2C). The de cha f Y139$^{G\ 2}$ f a h d ge b d h he a cha f P733^{Wh} (F g. 2C). N100$^{G\ 2}$ a d R136$^{G\ 2}$ f a h d ge b d a d a a b dge h he a cha a d de cha f E737^{Wh} , e ec e (F g. 2D). D81$^{G\ 2}$ f add a e ec a c e ac h R739^{Wh} (F g. 2D). I h d be e ed ha he h d h b c e ac be ee L741^{Wh} a d L18/A21/L22/F40/A56/I57 f G 2^{TPR} f he ab e he c e a e b (F g. 2E). C- e , a ha d he e a e ac ea e ed e e ab hed he G 2^{TPR}-Wh^{GBD} e ac ITC-ba ed a a (F g. 2F). I a c a , b f E732 f Wh^{GBD} h A a a ab hed he e ac (F g. 2F), gge g ha E732 e e a f he e ac , h ch e a h Wh$^{734\ 746}$ d d e ac h G 2^{TPR} he GST -d a a (F g. 1C). N ab e d e Wh^{GBD} ha c b e he e face a e ab e c e ed a g d ffe e ec e (F g. 2G), g he d e ab e f c f he G 2-Wh c e h gh- he e .

Gpsm2 undergoes phase separation inliv0.00cells.158 Gpsm1 under0

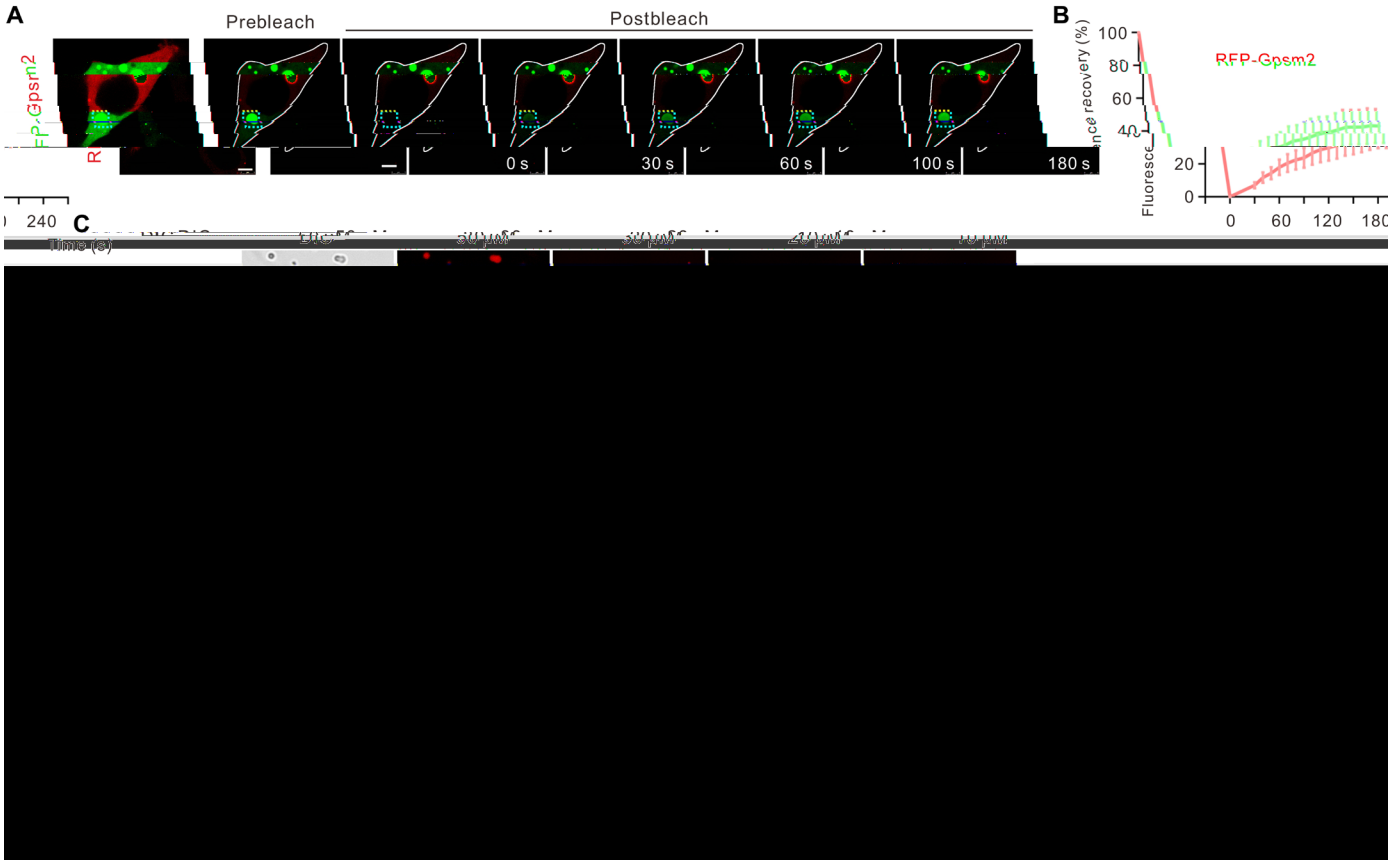

Fig. 3. Gpsm2 undergoes phase separation in vitro and in living cells. (**A**) Representative images showing expression of RFP-Gpsm2 in human embryonic kidney (HEK) 293T cells produced many spherical puncta. FRAP experiments showing that RFP-Gpsm2 signals recovered quickly after photobleaching within a short period of time. The photobleached area is indicated with a yellow dotted box. Scale bar, 5 μm. (**B**) Quantitative results for FRAP experiments of RFP-Gpsm2 in puncta and cytoplasm of HEK293T cells. Time 0 refers to the time point of the photobleaching pulse. All data are represented as means ± SEM from five droplets ($n = 5$) in cells. (**C**) Representative DIC and fluorescence images showing that purified full-length Gpsm2 protein underwent phase separation at indicated concentrations. Gpsm2 was sparsely labeled by Cy3 at 1%. Scale bar, 5 μm. (**D**) Representative images showing the Gpsm2 liquid-like droplets (indicated by arrows) fused with each other over time. Scale bar, 1 μm. (**E**) Fluorescence images showing that the number of the Gpsm2 droplets were reduced with increased NaCl concentration. Scale bar, 5 μm. (**F**) Schematic diagram showing the domain organization of Gpsm2. The deafness-associated mutation Gpsm2^{R318RfsX8} was also indicated. Note that there is a lysine-rich region (poly-K loop) in the linker region between TPR and GL domains. (**G**) The percentage of cells showing spherical puncta with various Gpsm2 constructs. All data are expressed as means ± SEM. Five batches of cultures with 30 cells counted in each batch.

h g fG 2, a h gh he e ha e h gh c e ed f c a d a (f g. S3). G e he e a e f he -K LLPS, AGS3, h ch ac h e e ce, d d f LLPS a e ec ed (F g. 3G).

A CMCS-associated mutation interferes with Gpsm2 LLPS

N ab a a f *Gpsm2*, .R318Rf X8, a f d a e h CMCS (*23*). .R318Rf X8 e c de a ca ed e ac g he -K a d a f GL f (F g. 3F). Beca e e e e ed f LLPS a e g h ca ed e, G 2$^{R318Rf X8}$ fa ed f LLPS a e ec ed (F g. 3G).

Cocondensation of Gpsm2 and Whirlin

We ece h ed ha Wh c d f ha e- e a a ed c - de a b h a d g ce (*14*). Beca e G 2 h - ca e ac h Wh , e e de ed he he G 2 c de a e a d he Wh c de a e ca c e h each he. G ee f e ce e (GFP) Wh e fec c ca ed h RFP-G 2 he b gh c a he he e e c e ed h - a e b c d e (HEK) 293T ce (F g. 4A). B h GFP a d RFP g a he c a c d ec e af e h b each g h a h e d f e (F g. 4B). We a f d ha g e a a f C5- abe ed G 2 a d C3- abe ed Wh ga e e c de ed d- ec d e (F g. 4C). FRAP a - a h ed ha b h e c d e cha ge be ee he c - de ed ha e a d he a e , a h gh he ec e a e e e ha h e ce (F g. 4D). C ec e , he e e d ca ed ha G 2 a d Wh c d f c c de a e b h a d ce .

Reconstitution of 5xTCD condensates

M 15, E 8, Wh , G 2, a d Gα e ac h each he f af e-c e c e ec f c he a e e e c a (F g. 1B). Th , e ea ab h he ed ha M 15, E 8, a d Gα c d be ec ed he G 2-Wh c c de a e be- ca e f he e ac e . We ed e f h b

Downloaded from https://www.science.org at Shanghai Jiao Tong University on June 23, 2022

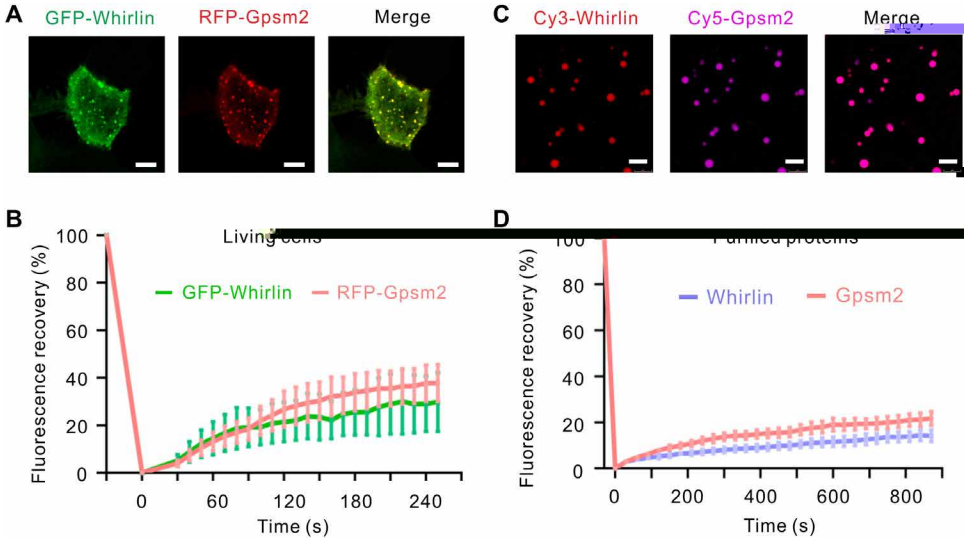

Fig. 4. Cocondensation of Gpsm2 and Whirlin. (**A**) Representative images showing coexpression of GFP-Whirlin and RFP-Gpsm2 in HEK293T cells produced many

ec f he f e-c e c e . We e ab e f a he e e ce f - e gh M 15 (*14*). I ead, e cce f f ed a ca ed f f M 15 (.e., C- e a a h g 4 4.1/e / ad / e PDZ b d g f, a ac d 2972 3511) ha c de b h b d g e f Wh a d E 8 (F g. 1B) (*14*). I he f g ec a a , e efe h ca ed e a M 15^{CTD}. N ab a h gh e e ab e f f - e gh E 8 (E 8^{FL}), h e e , hea f E 8^{FL} a e a e ed, h ch ab e f e e ha e a a d I ead, e e ab e b a a ge a f a ca ed E 8 (E 8^{NTD}; F g. 1B) h ch c de he b h b d- g e f Wh a d M 15. N ab E 8^{NTD} a d E 8^{FL} h ed c a ab e effec a e b f TCD c de a e (f g. S4). The e- f e, e ed E 8^{NTD} he f g ec a a , h ch a acc da ce h e (*14*). A he - e ed he ec a a e e f e h f ed a d be- ha ed e (f g. S5).

We e ded d LLPS f he f e-c e c e g ab e ed e de f e ce ce c c H e e , beca e f he a f he f e ce ce c c ech g e e e e ab e a e ab e f e a a e. The ef e, e dec ded a f d ffe e c b a f he f ec - e . F , e ch e ab e M 15^{CTD} f c d be ec ed he Wh c de a e ge he h E 8^{NTD} e d (*14*). Whe g f e ce ab e ed E 8^{NTD} (A e a F 488), Wh (C 3), G 2 (C 5), a d Gα_3 (A e a F 405) a a 1:1:1:1 a a a he d d a c ce a f 5 μM, e ead b- e ed c e e - ed, d- ha e d e h he ca ha e de f e ce ce c c (F g. 5A). The , e ch e ab e Wh a d f d ha E 8^{NTD} (A e a F 488), M 15^{CTD} (C 3), G 2 (C 5), a d Gα_3 (A e a F 405) f ed c d e a e (F g. 5A). F e ce ce age h ed ha each d e a h gh e ched h each c e f he c e (F g. 5A). The e da a g d ca ed ha he f e-c e c e ca f d- ha e c de a . T f he e f h , e ea ed he 5 TCD c de a e h 1,6-he a ed , h ch ha bee de ed f LLPS d. T ea e f 1,6-he a ed g ea a ed he LLPS (F g. 5B), d ca g he e e b e cha- ac e f he 5 TCD c de a e . F a ff e-c e c e c de a e a h gh ec f c a he ca f c- d e ha e a ed e , h ed (T) (f g. S6).

Gpsm2-Gα*i* significantly promotes LLPS of Whirlin-Myo15^{CTD}-Eps8^{NTD} condensates

Beca e b h Wh -M 15^{CTD}-E 8^{NTD} (3 TCD) c de a e a d 5 TCD c de a e f ed a LLPS, e e ded - e a ca c a e he ha e e a a ab e a g 3 TCD, 4 TCD$^{G\ 2}$ (G 2-Wh -M 15^{CTD}-E 8^{NTD}), 4 TCD$^{G\alpha\ 3}$ (Gα_3-Wh -M 15^{CTD}-E 8^{NTD}), a d 5 TCD c de a e . We f d ha add f G 2 (b Gα_3) he 3 TCD g f- ca c ea ed he be f d- e d e (F g. 5C). F - he add f Gα_3 he e g 4 TCD$^{G\ 2}$ d f he c ea e he be (F g. 5C). I add , e a c a ed he h eh d c ce a f LLPS a g d ffe e c e e . A e de a ed e (*14*), E 8^{NTD} a ea d E 8^{NTD}-M 15^{CTD} c e d d f LLPS e e a he d d a c ce a f 30 μM. The 3 TCD f ed LLPS a he d d a c ce a- f 5 μM, h e 4 TCD$^{G\ 2}$ (b 4 TCD$^{G\alpha\ 3}$) a d 5 TCD f ed LLPS a ch e h eh d c ce a f 1 μM (F g. 5D). The e da a gge ed ha G 2, b Gα_i e ha ced LLPS f 3 TCD. The effec e d e he ha e e a a f G 2, a a f G 2 (.e., G 2^{KA} a d G 2$^{R318Rf\ X8}$) ha a ed he LLPS f G 2 a h ed defec a e b f 5 TCD c de a e (F g. 5, C a d D). C - e , Gα_i d d f LLPS b (f g. S7). I h d be ed ha he h eh d c ce a f 5 TCD a c e

Fig. 5. Gpsm2-Gα*i* significantly promotes formation of the five-component tip complex condensates. (**A**) Representative fluorescence images showing that mixture of Whirlin, Myo15^{CTD}, Eps8^{NTD}, Gpsm2, and Gα_{i3} at their individual concentration of 5 μM led to formation of the liquid-like codroplets. Top: Whirlin, Eps8^{NTD}, Gpsm2, and Gα_{i3} were labeled with Cy3, Alexa Fluor 488, Cy5, and Alexa Fluor 405, respectively, with each at 1% level. Bottom: Myo15^{CTD}, Eps8^{NTD}, Gpsm2, and Gα_{i3} were labeled with Cy3, Alexa488, Cy5, and Alexa405, respectively, with each at 1% level. Scale bar, 5 μm. (**B**) Treatment of 1,6-hexanediol greatly impaired the LLPS of the 5xTCD condensates. Scale bar, 5 μm. The concentration of each component was 15 μM. (**C**) Quantification data of the number of the liquid-like droplets formed by 3xTCD (Whirlin-Myo15^{CTD}-Eps8^{NTD}), 4xTCD^{Gpsm2} (Gpsm2-Whirlin-Myo15^{CTD}-Eps8^{NTD}), 4xTCD^{Gαi3} (Gα_{i3}-Whirlin-Myo15^{CTD}-Eps8^{NTD}), wild-type 5xTCD condensates, and 5xTCD with Gpsm2 mutations (i.e., Gpsm2^{KA} mutant and Gpsm2^{R318RfsX8} mutant). Data were presented as means ± SEM from three independent experiments (six fields for each experiment) using Student's *t* test (****$P < 0.0001$; ns, not significant). (**D**) Phase separation diagram of different tip complex components at indicated concentrations. Highlighted red dots, phase separation; gray dots: no phase separation.

e e e ha 1 μM, gge g ha he 5 TCD c de a e a f a he h g ca c d .

5xTCD condensates induce robust actin bundling

H ca he 5 TCD c de a e c b e add a ac e - ga a he a e e e c a? We a ed e ga e he c e a be ee he TCD c de a e a d ac c e e d a c. T h e d, e ca ed he ac -b d g e - e he e e ce f a TCD c de a e (F g. 6A). We ed E 8^{FL} he e beca e E 8^{CTD} ece a f ac b d g (F g. 1B) (*33*). The ef e, E 8 ed he f g ac b d g e e e a f - e g h f . A e ec ed, E 8^{FL} a ec d d ce ac b d g, a h gh h ad c ac b d e (F g. 6A). Add f M 15^{CTD} E 8^{FL} d d cha ge he ac ch (F g. 6, A a d B). The 3 TCD c de a e g f ca d ced e b d ed ac f a e, a de c bed e (*14*). C e h he ha e e a a ab e (F g. 5, C a d D), 4 TCD^{G} ^{2}c de a e e h b ed ch ge ac - b d g ab ha 3 TCD c de a e d d, h e 5 TCD c de a e d - a ed a ab a 4 TCD^{G} ^{2}c de a e d d (F g. 6, A a d B). M e e, e ed a e ec c c (TEM) d ec a e ac b d e he e e ce f he c e c de a e. I e h he b e a f e ce c c a a, h c e ac b d e e e b e ed de TEM he 5 TCD 4 TCD^{G} ^{2}c de a e e e added he e ha h e 3 TCD c de a e (F g. 6, C a d D). The f e-c e c e

Downloaded from https://www.science.org at Shanghai Jiao Tong University on June 23, 2022

f ed c d e a he d d a c ce a c e d g h e he ac -b d g a a (f g. S8). The 5 TCD c - e c ca ed a c ec e c a a g h F-ac b d e (F g. 6E), gge g ha he 5 TCD c de a e a ac a g he F-ac b d e. T f he e ha he b ac - b d g ac f he 5 TCD c de a e a

Downloaded from https://www.science.org at Shanghai Jiao Tong University on June 23, 2022

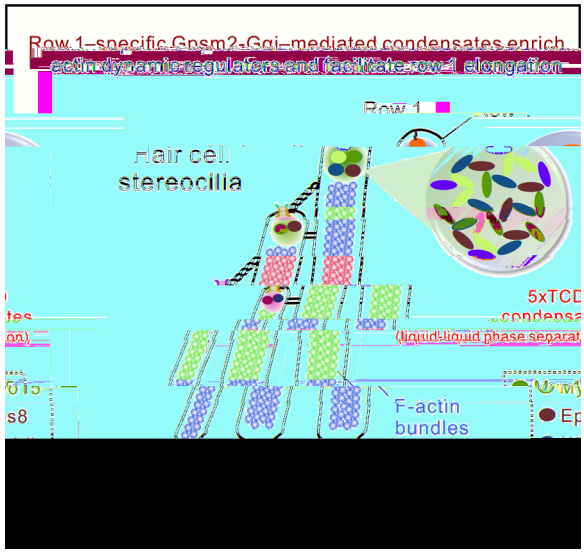

Fig. 7. A model depicting that row 1–specific Gpsm2-Gαi–mediated condensates enrich actin dynamic regulators and facilitate row 1 elongation. In the developing stereocilia, Gpsm2-Gαi is restrictedly transported to the tips of the tallest stereocilia where they form a five-component complex with Whirlin-Myo15-Eps8. Gpsm2-Gαi notably promotes the 5xTCD condensates that, in turn, effectively enrich actin dynamic regulators (including but not limited to Eps8 and Myo15) and facilitate robust actin elongation at the tips of the tallest stereocilia. In contrast, shorter rows are unable to generate stereocilia with a comparable height, most likely because of lack of Gpsm2-Gαi that leads to weakened phase separation ability and actin elongation capability.

Downloaded from https://www.science.org at Shanghai Jiao Tong University on June 23, 2022

e deg ada e . I e ha acc a f 1 ec f c e ead f a f TCD c de a e ha e b ac e ga e e , h e ed c f - e e ed LLPS a d b e e he e ga ce . We de a d ha d ec e ga f he TCD c de a e ha ce cha e g g a c e age beca e f ech ca , a d f e def e eeded de a e he c - ca e e e c a de e e . Ne e he e , de a f f c ce ha c de a f 1 ec f c c e a LLPS a de e ha b d e de

MATERIALS AND METHODS

Protein expression and purification

The c d g e e ce f Wh (Ge Ba : AB040959.1), G 2 (Ge Ba : NM_029522.2), AGS3 (Ge Ba : NM_001355574.1), Gα$_3$ (Ge Ba : NM_006496.3), M 15 (Ge Ba : NM_010862.2), a d E 8 (Ge Ba : NM_007945.3) e e c ed a e de c bed d f ed ET32a ec h a T ag a d a H$_6$- ag a N e (*14*). P e fa c c a e ed ab e S2. F he GST -d a a , a f ag e f Wh e e c ed he GEX-4T-1 ec . M a e e c ea ed h gh e- d ec ed age e e h d a d c f ed b DNA e e c g. A c c e e e ed *Escherichia coli* BL21 (DE3) (T a ge B ech; ca a g . CD601) C d P (We d B ; ca a g . EC1007) h ce a 16 C f 18 h d ced b 0.2 M - β-D- h ga ac de (f a c ce a). Rec b a e e f ed a e de c bed (*14*). I ge e a , H$_6$- agged a d GST- agged e e e f ed b N^{2+} ace c ac d aga- eaff ch a g a h a d GSH [g a h e (ed ced f)] e ha eaff ch a g a h , e ec e E ed a ge e e e f he f ed b a e e c ch a g a h (SEC) (H L ad 26/600 S e de 200 g, C a) he b ffe f 50 M (H 8.0), 300 M NaC , 1 M d h h e (DTT), a d 1 M EDTA. F he ec f he c e , H - agged - e e e c ea ed b h a h 3C ea e a 4 C e- gh a d he f ed b a he e f SEC f ca .

ITC assay

ITC a a e e e f ed a M c Ca TC200 e (Ma e Pa a ca , UK) a 25 C. Va G 2^{TPR} a d Wh ^{GBD} f ag- e e ed ed he b ffe c a g 50 M (H 8.0), 100 M NaC , 1 M EDTA, a d 1 M DTT. The Wh ^{GBD} - e (500 μM) e e aded ge, a d he G 2^{TPR} - e (50 μM) e e aded he ce . I each a , 2-μ a f e he ge a ec ed he ce , a d he e e a a 120 a e e ha he a ea e ed he ba e e. T a da a e e f ed h he e- e b d g de g O g 7.0.

GST pull-down assay

F e h f ed H$_6$-G 2^{TPR} a c ba ed h a f f GST-Wh f ag e f 1 h a 4 C. Af e ce f ga f 10 a 4 C, he e a a a aded 30-μ GSH- e ha e 4B bead c ba e f 30 a 4 C. Af e a h g h PBS b ffe h ee e , he b d e e e ed b b g h 30 μ f 2 SDS ac a de ge e ec h e ad g d e a d de ec ed b We e b ga -H a b d (Sa - fe ce ce , ca a g . SLAB28; 1:5000).

Crystallization, data collection, and structure determination

T b a ab e G 2^{TPR}-Wh ^{GBD} c e , G 2^{TPR} (a ac d 15 350) a f ed h Wh ^{GBD} (a ac d 717 746). The be c a f he f e (10 g/) e e b a ed b he ha g g d ff e h d a 16 C he b ffe c a - g 1.2 M a a a ed ba ca d 0.1 M (H 8.8). C - a e e c ec ed he c e d g e e h 25% g ce bef e - a d ff ac e e e . The d ff ac da a e e c ec ed a BL41XU a S g-8 (H g , Ja a). The d f- f ac da a e e ce ed h XDS (*40*). The c e c e a ed b he ec a e ace e e h d g he c- e f GPSM2^{TPR} G 2-N MA c e (P e Da a Ba c de: 3RO2) a he ea ch g de h gh he f a e f Pha e (*41*). F he ef e e a e f ed g Phe (*42*) a d C (*43*). The f a ef e e a c f he c e c e a e ed ab e S1. S c a d ag a e e e a ed b P MOL.

Protein labeling with fluorophore

F e h f ed agged e e e abe ed a de c bed e (*14*). I ge e a , e e e f d ed he b ffe c a g 300 M NaC , 100 M NaHCO$_3$ (H 8.3), a d 4 M β- ec a e ha (β-ME). C -3/C 5 *N*-h d cc de (NHS) e e (AAT B e ; ca a g . 271/280) a d A e a F 405/488 NHS e e (The F he Sc e f c; ca a g . A30000/A20000) e e d ed d- e h f de a d c ba ed h he d ca ed e (a a f 1:1) a e e a e f 1 h . The abe g eac a e ched b add f he b ffe f 200 M (H 8.2). The e a he f ed h a H T a de a g c h he b ffe c a g 50 M (H 8.0), 300 M NaC , a d 4 M β-ME e e he abe ed f h e. F ece ce abe g eff- ce c a de e ed b Na D 2000 (The F he Sc e f c).

In vitro phase separation assay

A f e h f ed a d abe ed e e e d ed he b ffe c a g 50 M (H 8.0), 300 M NaC , a d 4 M β-ME. Af e ce f ga a 16,873*g* f 10 a 4 C, a e e e aced ce bef e he ha e e a a a a . Each ha e e a a a e a ade b g f d ca ed abe ed e a d ca ed c- ce a f 10 a 25 C. Each a e a he ec ed a h e ade cha be a de c bed e (*44*) f f ece ce ag g (Le ca TCS SP8).

FRAP assay

FRAP a a a e f ed a e de c bed (*14*). I b ef, he a a a ca ed a Le ca SP8 c f ca c c e. F C 3- abe ed e d e , ac c a eg f e e (ROI) a b eached b a 561- a e bea a e e a e. F FRAP a a d- ha ed e gce , HEK293T ce (A e ca T e C e C ec ; ca a g . CRL-3216; Re ea ch Re ce Ide f e : CVCL_0063) e e c ed ga -b d he (Ma Te) a d a fec ed h he d ca ed a d . GFP a d RFP g a e e b eached h 488- a d 561- a e bea a 37 C, e ec- e F each e e e , he f ece ce e f a e ghb - g d e h a e he b eached e a a ec ded f e c ec . Bac g d e a b ac ed bef e da a a a . The ROI e a e 0 (gh af e he h - b each g) a e a 0%, a d he eb each g e a a - ed 100%.

Downloaded from https://www.science.org at Shanghai Jiao Tong University on June 23, 2022

Actin-bundling assay

T b a ea e b ed F-ac f a e , e c abb G-ac (C e e) a d ced e ef 1 h a e ea- e he e a b ffe c a g 50 M (H 8.0), 1 M ade e 5 - h ha e, 0.5 M DTT, 0.2 M CaC_2, 2 M MgC_2, a d 50 M KC . F e h f ed d- e a d a f ff e-c e c e ea d he c e e h- G 2-Gα_3 e e c ba ed h he ab e ea e b ed F-ac (2 μM) a e e a ef 1 h . Ac a he abe ed h h da e- ha d e (C e e) f 15 . The a e e ca ef ed be ee a de a d a c e a d aged b f e ce ce c c (Le ca TCS SP8). I he e a a , he c ce - a f each c e a h a af : E 8^{FL}, 0.25 μM; Wh , 0.5 μM; M 15^{CTD}, 0.5 μM; G 2 WT/ a , 0.5 μM; Gα_3, 0.5 μM; F-ac , 2 μM.

Sa e f TEM (Tec a G2 S 120 V) e e ad bed g -d cha ged, ca b -c a ed f a f c e g d f 1 a d ega e a ed h 0.75% (/) a ace a e f 45 . The c ce a f each c e h a a a h a f : E 8^{FL}, 0.25 μM; Wh , 1 μM; M 15^{CTD}, 1 μM; G 2 d e/ a , 1 μM; Gα_3, 1 μM; F-ac , 2 μM.

Statistical analyses

A a c [e.g., be f a e (*n*) a d b g ca e ca e (*N*) f a e e e] e e de c bed he f g e ege d . A da a e e e e ed a ea + SEM g he - a ed S de ' *t* e , g G a hPad P . A e e e e e f ed a ea h ee e de e de .

SUPPLEMENTARY MATERIALS

Supplementary material for this article is available at https://science.org/doi/10.1126/sciadv.abn4556

View/request a protocol for this paper from *Bio-protocol*.

REFERENCES AND NOTES

1. P. G. Gillespie, U. Muller, Mechanotransduction by hair cells: Models, molecules, and mechanisms. *Cell* **139**, 33–44 (2009).
2. P. G. Barr-Gillespie, Assembly of hair bundles, an amazing problem for cell biology. *Mol. Biol. Cell* **26**, 2727–2732 (2015).
3. B. Kachar, M. Parakkal, M. Kurc, Y. Zhao, P. G. Gillespie, High-resolution structure of hair-cell tip links. *Proc. Natl. Acad. Sci. U.S.A.* **97**, 13336–13341 (2000).
4. G. P. Richardson, C. Petit, Hair-bundle links: Genetics as the gateway to function. *Cold Spring Harb. Perspect. Med.* **9**, a033142 (2019).
5. D. N. Furness, C. M. Hackney, Cross-links between stereocilia in the guinea pig cochlea. *Hear. Res.* **18**, 177–188 (1985).
6. C. L. Cunningham, U. Muller, Molecular structure of the hair cell mechanoelectrical transduction complex. *Cold Spring Harb. Perspect. Med.* **9**, (2019).
7. A. K. Rzadzinska, M. E. Schneider, C. Davies, G. P. Riordan, B. Kachar, An actin molecular treadmill and myosins maintain stereocilia functional architecture and self-renewal. *J. Cell Biol.* **164**, 887–897 (2004).
8. M. M. Mogensen, A. Rzadzinska, K. P. Steel, The deaf mouse mutant whirler suggests a role for whirlin in actin filament dynamics and stereocilia development. *Cell Motil. Cytoskeleton* **64**, 496–508 (2007).
9. I. A. Belyantseva, E. T. Boger, S. Naz, G. I. Frolenkov, J. R. Sellers, Z. M. Ahmed, A. J. Griffith, T. B. Friedman, Myosin-XVa is required for tip localization of whirlin and differential elongation of hair-cell stereocilia. *Nat. Cell Biol.* **7**, 148–156 (2005).
10. V. Zampini, L. Ruttiger, S. L. Johnson, C. Franz, D. N. Furness, J. Waldhaus, H. Xiong, C. M. Hackney, M. C. Holley, N. Offenhauser, P. P. Di Fiore, M. Knipper, S. Masetto, W. Marcotti, Eps8 regulates hair bundle length and functional maturation of mammalian auditory hair cells. *PLOS Biol.* **9**, e1001048 (2011).
11. H. W. Lin, M. E. Schneider, B. Kachar, When size matters: the dynamic regulation of stereocilia lengths. *Curr. Opin. Cell Biol.* **17**, 55–61 (2005).
12. F. J. Probst, R. A. Fridell, Y. Raphael, T. L. Saunders, A. Wang, Y. Liang, R. J. Morell, J. W. Touchman, R. H. Lyons, K. Noben-Trauth, T. B. Friedman, S. A. Camper, Correction of deafness in shaker-2 mice by an W.

33. A. Disanza, M. F. Carlier, T. E. Stradal, D. Didry, E. Frittoli, S. Confalonieri, A. Croce, J. Wehland, P. P. Di Fiore, G. Scita, Eps8 controls actin-based motility by capping the barbed ends of actin filaments. *Nat. Cell Biol.* **6**, 1180–1188 (2004).
34. A. Rzadzinska, M. Schneider, K. Noben-Trauth, J. R. Bartles, B. Kachar, Balanced levels of Espin are critical for stereociliary growth and length maintenance. *Cell Motil. Cytoskeleton* **62**, 157–165 (2005).
35. P. A. Loomis, L. Zheng, G. Sekerkova, B. Changyaleket, E. Mugnaini, J. R. Bartles, Espin cross-links cause the elongation of microvillus-type parallel actin bundles in vivo. *J. Cell Biol.* **163**, 1045–1055 (2003).
36. Z. G. Moreland, F. Jiang, C. Aguilar, M. Barzik, R. Gong, A. Shams, C. Faaborg-Andersen, J. C. Werth, R. Harley, D. C. Sutton, S. M. Cole, A. Parker, S. Morse, E. Wilson, Y. Takagi, J. R. Sellers, S. D.M. Brown, T. B. Friedman, G. M. Alushin, M. R. Bowl, J. E. Bird, Myosin-driven nucleation of actin filaments drives stereocilia development critical for hearing. bioRxiv 2021.07.09.451618 [Preprint] 13 July 2021. https://doi.org/10.1101/2021.07.09.451618.
37. F. S. Willard, Z. Zheng, J. Guo, G. J. Digby, A. J. Kimple, J. M. Conley, C. A. Johnston, D. Bosch, M. D. Willard, V. J. Watts, N. A.

ScienceAdvances

Promotion of row 1–specific tip complex condensates by Gpsm2-G#i provides insights into row identity of the tallest stereocilia

Yingdong ShiLin LinChao WangJinwei Zhu

Sci. Adv., 8 (23), eabn4556. • DOI: 10.1126/sciadv.abn4556

View the article online
https://www.science.org/doi/10.1126/sciadv.abn4556
Permissions
https://www.science.org/help/reprints-and-permissions

Downloaded from https://www.science.org at Shanghai Jiao Tong University on June 23, 2022

Use of this article is subject to the Terms of service

Science Advances (ISSN) is published by the American Association for the Advancement of Science. 1200 New York Avenue NW, Washington, DC 20005. The title *Science Advances* is a registered trademark of AAAS.
Copyright © 2022 The Authors, some rights reserved; exclusive licensee American Association for the Advancement of Science. No claim to original U.S. Government Works. Distributed under a Creative Commons Attribution NonCommercial License 4.0 (CC BY-NC).